Optimization of Three-Terminal Perovskite/Silicon Tandem Solar Cells

Santbergen, Rudi; Uzu, Hisashi; Yamamoto, Kenji; Zeman, Miro

DOI
10.1109/JPHOTOV.2018.2888832

Publication date
2019

Document Version
Accepted author manuscript

Published in
IEEE Journal of Photovoltaics

Citation (APA)
Santbergen, R., Uzu, H., Yamamoto, K., & Zeman, M. (2019). Optimization of Three-Terminal Perovskite/Silicon Tandem Solar Cells. *IEEE Journal of Photovoltaics*, *9*(2), 446-451. Article 8607100. https://doi.org/10.1109/JPHOTOV.2018.2888832

Optimization of Three-Terminal Perovskite / Silicon Tandem Solar Cells

Rudi Santbergen, Hisashi Uzu, Kenji Yamamoto, and Miro Zeman

***Abstract*—We use simulations to optimize perovskite / silicon tandem solar cells in a novel *three-terminal* configuration, with one terminal at the front and two at the rear. We consider configurations in which the top cell has either the inverted or the same polarity as the bottom cell. Our goal is to minimize the optical losses, to compare the performance of both configurations and to determine the realistically achievable efficiency. Optical simulations show that if the hole transporting material is in front of the perovskite it gives rise to parasitic absorption losses. If it is behind the perovskite, these losses are avoided, however at the cost of increased reflection losses. We systematically minimize these reflection losses. This increases the tandem's total implied photocurrent density from 34.4 to 41.1 mA/cm^2. To determine the corresponding power conversion efficiency of these three-terminal tandems, electrical circuit simulations are performed based on existing 22.7% efficient perovskite and 24.9% efficient silicon cells. These simulations show that tandem efficiencies up to 32.0% can be obtained.**

***Index Terms*—Photovoltaic cell, Light trapping, Perovskite, Tandem, Modeling, Equivalent circuit, Simulation.**

I. Introduction

ONE of the most promising routes towards low-cost solar cells with efficiencies over 30% is based on tandem solar cells with organometal halide perovskite top cell and crystalline silicon bottom cell [1-3]. Usually tandems with either two or four terminals are considered. The advantage of the *two-terminal* tandem is that lateral current collection (i.e. a transparent conductive layer) is not required at the rear of the top-cell and at the front of the bottom cell, resulting in potentially lower fabrication costs and higher efficiency [4]. On the other hand, an advantage of the *four-terminal* tandem is that no current matching is required, which allows a wider range of perovskite thicknesses and gives a higher spectral robustness. In this work we consider the less common *three-terminal* tandem, as originally proposed by Nagashima et al. [5], which combines the above mentioned advantages. We consider the three-terminal perovskite / silicon tandems as shown in Fig. 1. The silicon bottom cell is a conventional silicon heterojunction cell based on an n-type wafer passivated by thin layers of intrinsic or doped hydrogenated amorphous silicon (a-Si:H). At the rear it has interdigitated back contacts, which we name base and emitter contacts as indicated. The front side of the silicon cell is in electrical contact with the perovskite cell deposited on top. In the pn-np configuration the electron transporting material (ETM) is deposited first followed by perovskite and finally the hole transporting material (HTM), which is at the front. In the np-np configuration the top cell is inverted, with the HTM at the rear and ETM at the front. In this work we consider the HTM and ETM to be poly(tri-arylamine) (PTAA) and compact TiO_2, respectively. Indium doped tin oxide (ITO) serves as transparent front contact. Note that, as shown in Fig. 1, in the pn-np configuration, *electrons* generated in the top cell pass through the bottom cell to be collected in the base contact. The current collected by the base contact therefore is the sum of top and bottom cell currents. However, in the np-np configuration the *holes* generated in the top cell reach the tunnel recombination junction where they recombine with electrons generated in the bottom cell. Note that such a tunnel recombination junction is commonly used in two-terminal tandems. If the top cell generates the higher current ($J_{top} > J_{bot}$), there is an excess of holes at the junction. In that case the base contact *provides* electrons. However, if the bottom cell generates the higher current ($J_{bot} > J_{top}$), there is an excess of electrons and the base contact *extracts* electrons. Therefore, current can flow either into or out of the base contact. Both scenarios are indicated by dashed lines in Fig. 1 (right).

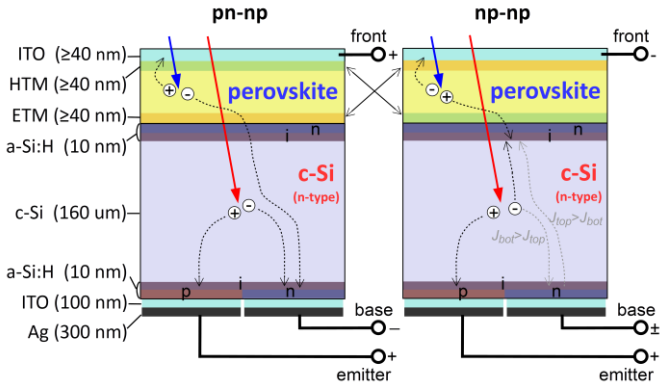

Fig. 1. Schematic cross-section of a 3-terminal perovskite/silicon tandem. Left: pn-np configuration. Right: np-np configuration.

Manuscript received December 4, 2018; accepted December 16, 2018; accepted April 18, 2018. Date of publication January 10, 2019; date of current version February 18, 2019.

R. Santbergen and M. Zeman are with Delft University of Technology, Mekelweg 4, 2628 CD, Delft, The Netherlands (e-mail: r.santbergen@tudelft.nl; m. zeman@tudelft.nl).

H. Uzu and K. Yamamoto are with Kaneka Corporation, 5-1-1 Torikai-Nishi, Settsu Osaka 566-0072, Japan (e-mail: kaneka.member@kaneka.co.jp; kenji.yamamoto@kaneka.co.jp).

Color versions of one or more of the figures in this paper are available online at http:// ieeexplore.org.

Digital Object Identifier 10.11109/JPHOTOV.2018.2888832

Today, the demonstrated record efficiency of single-junction silicon solar cells is 26.7% [9,10], while for perovskite cells this is 22.7%, albeit less stable and on a small 9 mm^2 area [11,12]. Both technologies have been combined successfully into perovskite / silicon tandems. Initially perovskite cells could be deposited only onto *flat* substrates. As a result, monolithic two-terminal tandems required flat top cell and reached efficiencies up to 23.6% [13, 14]. Recently, a two-step perovskite deposition process was developed that enables the top cell to be deposited onto a textured bottom cell. Such a two-terminal tandem has lower reflection losses and a higher efficiency of up to 25.2% [15]. Oxford PV recently reported a record efficiency of 27.3% [16]. Mechanically stacked *four*-terminal tandems have demonstrated efficiencies up to 26.9% [17,18]. An efficiency as high as 28.0% has been demonstrated for a device based on an optical splitting system [19]. So far, *three*-terminal perovskite / silicon tandems received less attention and to our knowledge have not been demonstrated experimentally [20]. Adhyaksa et al. simulate three-terminal perovskite / silicon tandems and conclude that these have an even higher efficiency potential than two- or four-terminal tandems [21]. That simulation study is however limited to the pn-np configuration and does not contain a detailed analysis of the optical losses.

In this work, we simulate the three-terminal perovskite / silicon tandems in detail. Our goal is to i) quantify and minimize optical losses, ii) compare the pn-np and np-np configurations, iii) determine tandem efficiencies as a function of perovskite thickness. Note that we are interested in tandem efficiencies achievable with proven technology. Our simulations will therefore be based on existing perovskite and silicon solar cells.

II. Methodology

A. Single Junction Reference Cells

As reference perovskite cell we take the 9 mm^2 cell made by KRICT with an initial efficiency of 22.7% (V_{oc} = 1144 mV, J_{sc} = 24.92 mA/cm^2, FF = 79.6%) [11,12]. The reference *silicon* solar cell is a six inch back contacted silicon heterojunction cell made by Kaneka Corporation with an efficiency of 24.9% (V_{oc} = 737 mV, J_{sc} = 42.13 mA/cm^2, FF = 80.2%) [22]. Note that this is not the record efficiency, but an efficiency realistically achievable in mass production. The measured *JV*-curves of the perovskite and silicon reference cells are shown in Fig. 2 as purple and orange circles, respectively.

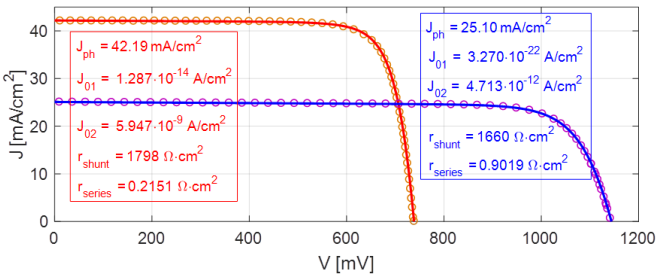

Fig. 2: Measured *JV*-curves of reference solar cells (circles) and best fit using single junction equivalent circuit model (lines). Perovskite data (purple) is taken from Ref. 11. Silicon data (orange) is taken from Ref. 22. The fit parameters of perovskite and silicon data are given as blue and red text, respectively.

B. Optical Simulation Method

The three-terminal tandems are optically simulated using the GenPro4 model developed at TU Delft [23]. The model calculates the absorptance in the top and bottom cell's absorber layer as a function of wavelength. By integrating this over the AM1.5g spectrum the implied photocurrent density J_{ph} of top and bottom cell are obtained. The model takes the effects of interference and surface texture into account. The thickness and complex refractive index $n + ik$ of every layer are given as input. The values of $n(\lambda)$ and $k(\lambda)$ are measured using ellipsometry and shown in Fig. 3. Note that n and k of perovskite are taken from Ref. 24 (blue dashed line) and then red-shifted by 15 nm to match the band edge of the EQE curve of the perovskite reference cell [11].

The layer thicknesses used in the optical simulation are given in Fig. 1. Interference effects are taken into account by simulating all thin layers coherently. The thickness of the ITO, HTM and ETM layers will be tuned to maximize the number of photons coupled into the perovskite and silicon absorber layers. Note that when parasitic absorption plays a role, this approach is more accurate than minimizing the number of reflected photons [25]. The thick silicon absorber layer does not give rise to interference and is modelled incoherently [23]. The thickness of the perovskite absorber layer will be varied between 50 and 1000 nm and for consistency it is also simulated incoherently for all thicknesses.

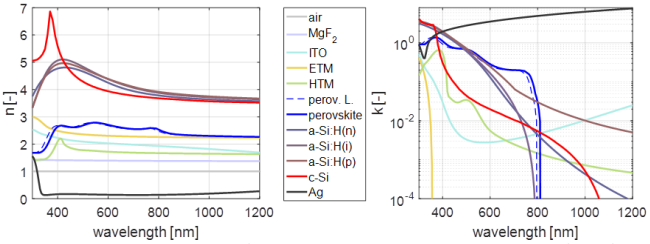

Fig. 3: Optical properties of layers used versus wavelength. Left: refractive index n. Right: extinction coefficient k.

C. Electrical Simulation Method

The *JV*-curve of solar cells can be reproduced by an equivalent electrical circuit with the following components: i) a current source characterized by a photo-current density J_{ph}, ii) two diodes, with ideality factors 1 and 2, characterized by saturation current densities J_{01} and J_{02} and iii) shunt and series resistances characterized by surface resistivities r_{shunt} and r_{series} [26]. If an experimental solar cell *JV*-curve is provided, the *JV*-curve of the circuit can be fit to this, using the parameters J_{ph}, J_{01}, J_{02}, r_{shunt} and r_{series} as a fit parameters. For example, an excellent fit can be found with the *JV*-curves of the single junction reference cells shown in Fig. 2 (solid lines). The corresponding fit parameters for the perovskite and silicon cell are shown as blue and red text, respectively.

The three-terminal pn-np and np-np tandems are represented by the equivalent circuits shown in Fig. 4. The parts indicated in blue and red represent the top and bottom cell, respectively. Note that the top and bottom cell are series-connected and share the base terminal. In the pn-np configuration the polarity of the top cell is inverted with respect to the bottom cell, while in np-np configuration top and bottom cell polarities are the same. The top and bottom cells' values of J_{01}, J_{02}, r_{shunt} and r_{series} are

assumed to be the same as for the single junction reference cells shown in Fig. 2. This means that for the perovskite top cell and silicon bottom cell, intrinsic efficiencies of respectively 22.7% and 24.9% are assumed. Note that the top and bottom cell absorb a different number of photons as part of the tandem compared to the corresponding single junction devices. This means that the top and bottom cell's J_{ph} values and therefore their *JV*-curves are different from the single junction curves given in Fig. 2. The top and bottom cell's J_{ph} values are calculated by the optical model (see section IIB) and used as input in the electrical simulation of the equivalent circuit shown in Fig. 4. The electrical circuit is simulated using the NGspice software [27]. The top cell's *JV*-curve is then obtained by sweeping the voltage between base and front contact and the bottom cells *JV*-curve is obtained by sweeping the voltage between base and emitter contact. Note that because top and bottom cell share the base resistor, top and bottom circuits are not entirely independent. Therefore the *top* cell's *JV*-curve is obtained while keeping the *bottom* cell at its maximum power point, and vice versa. To achieve this, the voltages of top and bottom cell are swept iteratively until this maximum power point is reached. From these *JV*-curves the corresponding top and bottom cell efficiencies are obtained. The tandem efficiency is the sum of top and bottom cell efficiency.

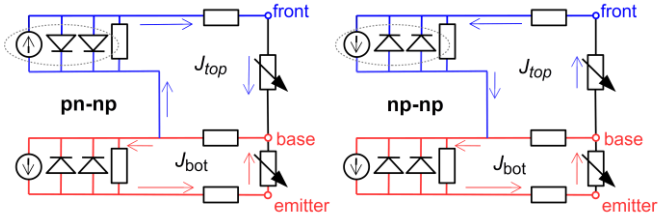

Fig. 4: Equivalent electrical circuit of three-terminal tandem. Left: pn-np configuration. Right: np-np configuration.

III. Optical Simulation Results

First in section IIIA the optical simulation results of the *standard* three-terminal tandem designs are presented. Then section IIIB introduces *enhanced* designs, in which reflection losses are reduced.

A. Standard design

In the standard design all interfaces are flat, i.e. without surface texture, as shown in Fig. 1. As mentioned in section IIB, the GenPro4 model is used to simulate this structure and tune the thicknesses of ITO, HTM and ETM layers in order to maximize incoupling of light. The number of photons coupled into perovskite is maximized by tuning the thickness of layers *in front of* the perovskite layer. For the pn-np configuration, the simulations show that incoupling into perovskite is maximized when the minimum thicknesses are used: ITO(40 nm) / HTM(40 nm). For the np-np configuration the less absorbing ETM is in the front and incoupling into perovskite is maximized for the following thickness combination: ITO(85 nm) / ETM(49 nm). Next, the number of photons coupled into the silicon is maximized by tuning the thickness of the layer directly *behind* the perovskite. Simulations show that in both configurations this is achieved with the minimum thicknesses, i.e. with 40 nm of ETM (in pn-np configuration) or 40 nm of HTM (in np-np configuration) behind the perovskite.

Having optimized the ITO, HTM and ETM thicknesses, the three-terminal tandems are simulated. Fig. 5 shows the simulated absorptance in every layer of the tandem as a function of wavelength. The left column shows the pn-np configuration and the right column shows the np-np configuration. From top to bottom, the perovskite thickness is increased from 50 to 200 and 1000 nm. The useful absorption in perovskite and silicon are indicated by the blue and red *line*, respectively. By integrating over the AM1.5g spectrum the corresponding implied photocurrent densities of top and bottom cell are obtained, which are indicated as blue and red text. There are also parasitic absorption losses, mainly in ITO (light blue area) and HTM (green area). In all cases there are significant reflection losses, indicated by the white area. Using the method described in Ref. 22, this loss is subdivided into reflection loss: R_1 from the interfaces in front of the perovskite layer, R_2 from the interfaces between perovskite and silicon layer, and R_3, from the interfaces behind the silicon layer.

Fig. 5 shows that with increasing perovskite thickness, absorptance in perovskite increases, at the cost of absorptance in silicon, as expected. The J_{ph} of the perovskite top cell and the silicon bottom cell increase and decrease correspondingly. Note that the tandem's total J_{ph}, i.e. the sum of perovskite and silicon J_{ph}, increases slightly with increasing perovskite thickness. This is because with increasing thickness, reflectance loss R_2 is reduced for wavelengths smaller than 800 nm.

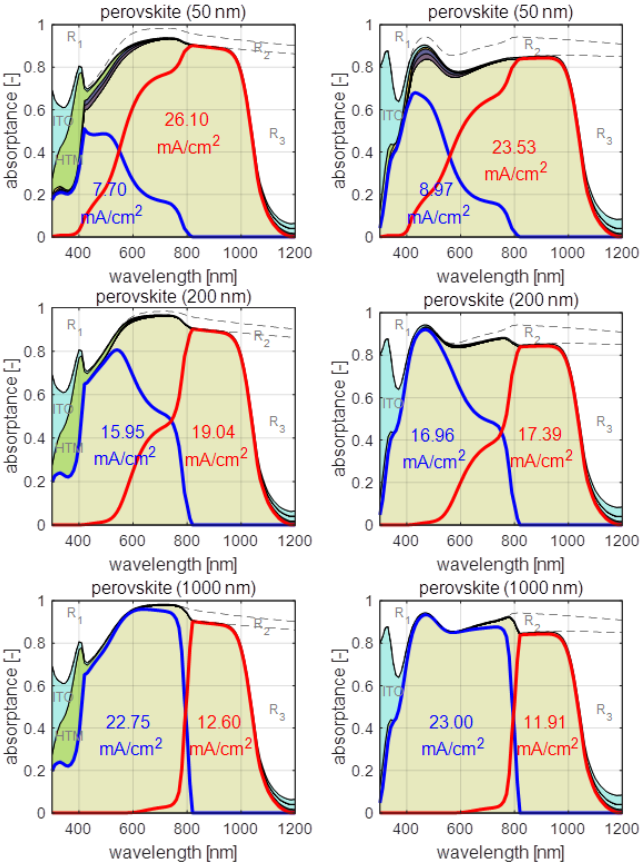

Fig. 5: Absorptance versus wavelength for every layer in the *standard* three-terminal perovskite / silicon tandem. White area indicates reflection losses. Left column: pn-np configuration. Right column: np-np configuration. Perovskite thickness: 50 nm (top), 200 nm (middle) and 1000 nm (bottom).

Comparing the np-np configuration (Fig. 5, right column) to the pn-np configuration (Fig. 5, left column) shows two main differences. Firstly, the np-np configuration, with the HTM *behind* the perovskite, does not suffer from parasitic absorption in the HTM, resulting in a higher J_{ph} for the perovskite top cell. Note that HTM, which in this case is PTAA, is only strongly absorbing for $\lambda < 450$ nm (see Fig. 3b) and in the np-np configuration this light is already absorbed in the perovskite before reaching the HTM. A similar conclusion was previously drawn for two-terminal tandems [28]. Secondly, the np-np configuration suffers from larger reflection losses. Especially reflection loss R_2 is larger. This results in a lower J_{ph} for the silicon bottom cell. This is caused by the relatively low index of HTM, compared to the neighboring layers (see Fig. 3a). Overall, at 200 nm perovskite thickness, the total J_{ph} of the pn-np configuration is 35.0 mA/cm^2, versus 34.4 mA/cm^2 for the np-np configuration. Note that the silicon single junction reference cell has a much higher J_{ph} of 42.2 mA/cm^2 (see Fig. 2). This indicates that there is much room to increase the total J_{ph} of the perovskite / silicon tandem, as will be investigated in the next section.

B. *Enhanced design*

In previous work we showed that reflection losses R_1, R_2 and R_3 can be reduced systematically by means of three anti-reflective measures: i) an additional front MgF_2 anti-reflective coating, ii) an interlayer between top and bottom cell and iii) a pyramid texture at the rear [29]. Here we consider so-called 'enhanced' tandem designs in which all three measures are implemented. Again both pn-np and np-np configurations are considered. We use optical simulations, first to optimize these enhanced tandem designs and then to determine the corresponding J_{ph} of top and bottom cell.

The first measure, adding the MgF_2 anti-reflective coating at the front, creates a triple-layer coating: MgF_2 / ITO / HTM (or ETM). As these thin layers give rise to interference, even a small variation in their thickness strongly affects the incoupling of light, just like in a triple-layer anti-reflective coating. Therefore a simplex search algorithm is used to find the thickness combination that maximizes the number of photons coupled into the perovskite. These simulations reveal that for the *pn-np* configuration, the optimum thickness combination is: MgF_2(115 nm) / ITO(40 nm) / HTM(40 nm). Note that both ITO and HTM are at their minimum allowed thicknesses, as this minimizes the parasitic absorption loss. For the *np-np* configuration, the optimum thickness combination is: MgF_2(107 nm) / ITO(70 nm) / ETM(54 nm). This shows that in this case using larger than the minimum ITO and ETM thicknesses is beneficial as parasitic absorption losses play a smaller role.

The second measure is adding an interlayer between top and bottom cell in order to maximize incoupling into the *silicon* absorber layer. For this interlayer we do not have a particular material in mind. Instead we let both the layer thickness and its refractive index be free parameters. We assume it to be non-absorbing in the relevant wavelength range. Note that this interlayer is sandwiched between the top cell's ETM or HTM layer, whose thickness we also treat as a free parameter, and the bottom cell's a-Si:H layers, whose thicknesses are kept fixed. A simplex search algorithm is used to find the parameter combination that maximizes the number of photons coupled into the silicon. Our simulations show that in the *pn-np* configuration, in which the interlayer is neighbored by the higher index ETM, the ideal interlayer has a refractive index of 2.85 and a thickness of 89 nm. In the *np-np* configuration, in which the interlayer is neighbored by the lower index HTM, the ideal the interlayer has a lower refractive index of 2.58, in combination with a larger thickness of 116 nm. A suitable material for this layer would be nc-SiO_x:H, as its refractive index can be tuned by varying the oxygen content [30,31]. This material has been used in tunnel recombination junctions before [32]. The simulations also show that the thickness of the neighboring ETM or HTM layer should be kept at the minimum value of 40 nm.

Finally, a so-called random pyramid texture is added. This type of texture is the widely used standard for mono-crystalline silicon solar cells. Note that the texture is added to only the rear side of the silicon wafer, as having a flat front side facilitates the deposition of the perovskite top cell [14]. In the simulations we use the texture's height profile obtained from atomic force microscopy and do not optimize this texture further.

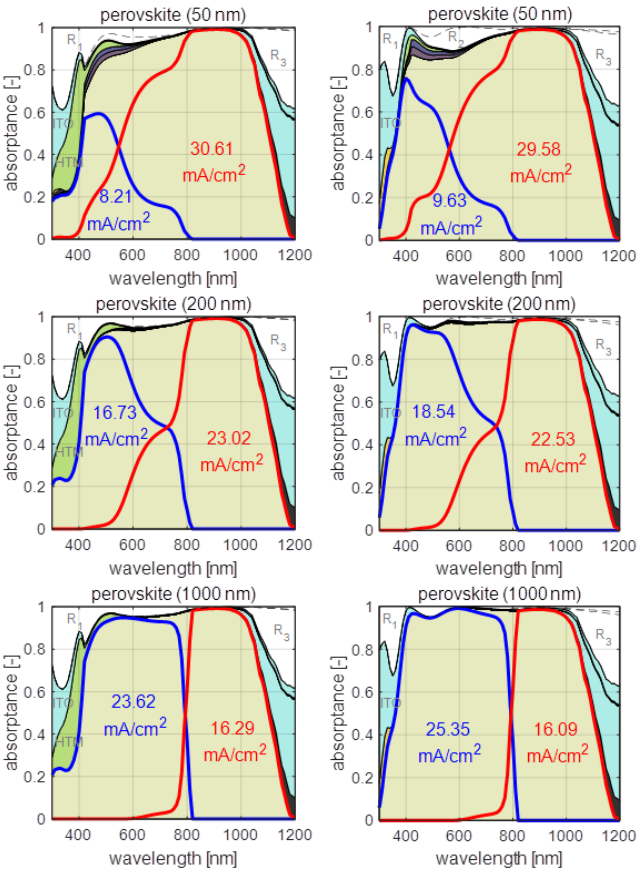

Fig. 6: Absorptance versus wavelength for every layer in the *enhanced* three-terminal perovskite / silicon tandem. White area indicates reflection losses. Perovskite thickness: 50 nm (top), 200 nm (middle) and 1000 nm (bottom). Left column: pn-np configuration. Right column: np-np configuration.

The simulation results of the *enhanced* three-terminal tandem with optimized MgF_2 coating, interlayer and rear texture are shown in Fig. 6. As before, pn-np and np-np configurations are shown in left and right columns,

respectively, with perovskite thickness increasing from 50 nm (top) to 200 nm (middle) and 1000 nm (bottom). The results show the same general trends as the standard designs (see section IIIA). The np-np configuration, with HTM behind perovskite, suffers less parasitic absorption loss, resulting in a higher J_{ph} for the top cell (compare left and right column Fig. 6). At the same time it suffers more reflection losses, resulting in a lower J_{ph} for the bottom cell. The main difference compared to the standard designs is that these enhanced designs have much reduced reflection losses (compare white areas in Fig. 5 and 6). As a result, the implied photocurrent densities of top and especially bottom cell have increased significantly. In our discussion we focus on the tandem with 200 nm thick perovskite layer. For the pn-np configuration top and bottom cell J_{ph} have increased by 0.8 and 4.0 mA/cm^2, respectively. For the np-np configuration the top and bottom cell J_{ph} have even increased by 1.6 and 5.1 mA/cm^2, respectively. The sum of top and bottom cell J_{ph}, is 39.8 mA/cm^2 for the pn-np configuration and as high as 41.1 mA/cm^2 for the np-np configuration. This shows that in terms of total J_{ph}, the np-np configuration can outperform the pn-np configuration, but only in the enhanced configuration where the reflection losses have been addressed.

IV. Electrical Simulation Results

The equivalent circuit model is used to calculate the corresponding tandem efficiencies (see section IIC). We use the J_{ph} of the top and bottom cell of the *enhanced* tandem designs, shown in Fig. 6, as input. The output of this simulation are the top and bottom cell's *JV*-curves, which are shown in Fig. 7 as blue and red lines, respectively. The results for the pn-np and np-np configurations are shown in the left and right columns, respectively and the perovskite thickness varies from 50 nm (top) to 200 nm (middle) and 1000 nm (bottom). The current, voltage and electrical power output at maximum power point are indicated for each case.

The most obvious trend in Fig. 7 is that with increasing perovskite thickness, the power output of the perovskite top cell increases at the cost of the power output from the silicon bottom cell, as expected. Compared to the pn-np configuration, the np-np configuration (right column) has a slightly lower power output from the silicon bottom cell, but a significantly higher power output from the perovskite top cell. So overall, the np-np configuration has the higher total power output. This is primarily because the np-np configuration has a higher total J_{ph}. A secondary effect is the fact that the ohmic losses in the base resistor are lower. The current flowing through this base resistor in pn-np configuration is the *sum* of top and bottom cell current, while for the np-np configuration it is only the *difference* (see Fig. 4).

The corresponding power conversion efficiencies are obtained by dividing the electrical output power densities by the power density of the incident light (100 mW/cm^2). Fig. 8 gives an overview of the perovskite top cell efficiencies (blue bars) and silicon bottom cell efficiencies (red bars) as a function of perovskite thickness. The pn-np and np-np configurations are shown in lighter and darker colors, respectively. The bars are stacked so that the tandem efficiency, the sum of both, can be identified. This shows that at 200 nm perovskite thickness, the np-np configuration has a 0.2% (absolute) lower silicon bottom cell efficiency, but a 1.8% (absolute) higher perovskite top cell efficiency and therefore has the higher tandem efficiency. This is also the case for 50 and 1000 nm perovskite thicknesses. For both pn-np and np-np configurations the tandem efficiency increases strongly with inreasing perovskite thickness. The highest efficiency, of as much as 32.0%, is obtained for the np-np configuration with 1000 nm thick perovskite layer.

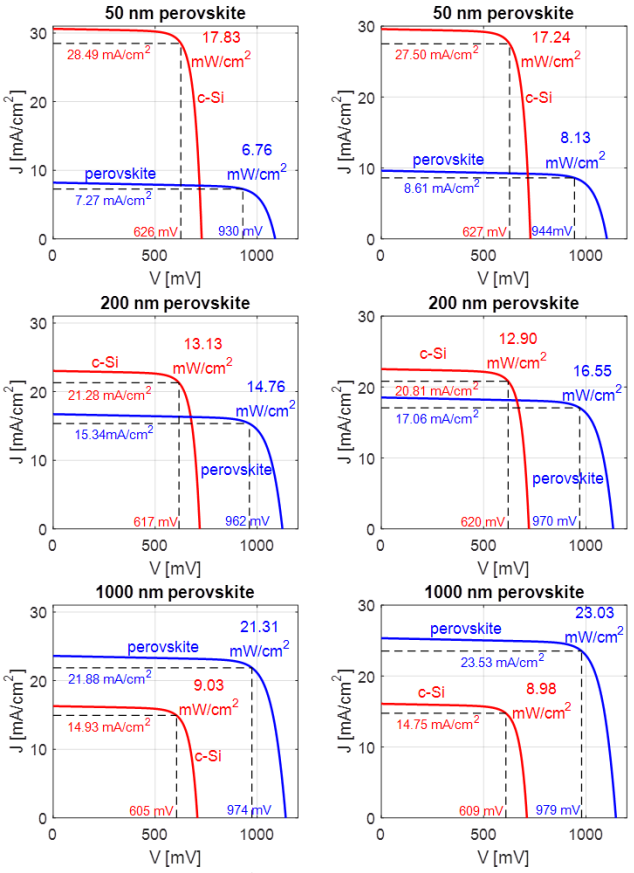

Fig. 7: Simulated *JV*-curve of perovskite top cell (blue) and silicon bottom cell (red). Perovskite thickness: 50 nm (top), 200 nm (middle) and 1000 nm (bottom). Left column: pn-np configuration. Right column: np-np configuration.

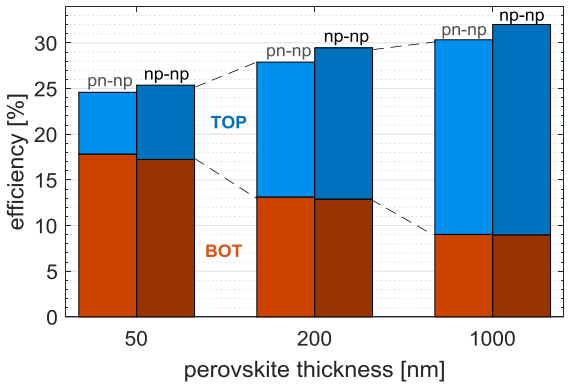

Fig. 8: Efficiency of perovskite top cell (blue) and silicon bottom cell (red) as a function of perovskite thickness. The lighter colors indicate the pn-np configuration and the darker colors indicate the np-np configuration.

As mentioned in the introduction, *three*-terminal tandems combine the advantages of conventional two- and four-terminal tandems. They suffer less parasitic absorption losses, as only one transparent conductive layer is required, and allow for a wide range of perovskite thicknesses. The simulations presented above show that these are essential requirements for maximizing the efficiency of perovskite / silicon tandems.

V. Conclusions

We use our GenPro4 optical model to optimize the design of three-terminal perovskite / silicon tandems. ITO, HTM and ETM layer thicknesses are tuned for maximum incoupling of light into the absorber layers. Optical simulations show that if the HTM layer is in front of the perovskite (in pn-np configuration) it gives rise to parasitic absorption losses at the smaller wavelengths. This reduces the J_{ph} of the perovskite top cell. If the HTM layer is behind the perovskite (in np-np configuration), these losses are avoided, however at the cost of increased reflection losses, especially in the near infrared. This reduces the J_{ph} of the silicon bottom cell. We systematically minimize the reflection losses by adding a front MgF_2 coating, an interlayer between top and bottom cell and a pyramid texture at the rear. When properly optimized, these additions increase the J_{ph} of top and bottom cell by as much as 1.6 and 5.1 mA/cm^2, respectively. The tandem's total J_{ph} thereby increases from 34.4 to 41.1 mA/cm^2.

To determine the corresponding efficiency of three-terminal tandems we use an equivalent circuit model. Input parameters are extracted from *JV*-measurements reported in literature. These simulations show that higher tandem efficiencies are obtained with thicker perovskite layers. Compared to the pn-np configuration, the np-np configuration has a slightly lower power output from the silicon bottom cell but a significantly higher power output from the perovskite top cell. Overall, the three-terminal perovskite / silicon tandem can reach efficiencies as high as 32%.

Acknowledgment

This work was supported in part by the New Energy and Industrial Technology Development Organization (NEDO) under the Ministry of Economy, Trade and Industry of Japan.

References and Footnotes

[1] M.A. Green, "Silicon wafer-based tandem cells: The ultimate photovoltaic solution?," *Proc. SPIE 8981, Physics, Simulation and Photonic Engineering of Photovoltaic Devices III*, 89810L (7 March 2014).

[2] M.A. Green, A. Ho-Baillie, and H.J. Snaith, "The emergence of perovskite solar cells," *Nature Photonics*, vol. 8, pp. 506-514, 2014.

[3] J. Werner, B. Niesen and C. Ballif, "Perovskite/silicon tandem solar cells: marriage of convenience or true love story? – An overview," *Advanced Materials Interfaces*, vol. 5, 1700731, 2018.

[4] M. Filipic *et al*., "CH3NH3PbI3 perovskite / silicon tandem solar cells: characterization based optical simulations," *Opt. Express*, vol. 23, A263-278, 2015.

[5] T. Nagashima, K. Okumura, K. Murata, and Y. Kimura, "Three-terminal tandem solar cells with a back-contact type bottom cell," *Conference record of the 28th IEEE PVSC*, 916102, 2000.

[6] Y. Jiang *et al.*, "Optical analysis of perovskite/silicon tandem solar cells," *J. Mater. Chem. C*, vol. 4, pp. 5679-5689, 2016.

[7] S. Albrecht *et al*., "Towards optical optimization of planar monolithic perovskite/silicon-heterojunction tandem solar cells," *J. Optics*, vol. 18, 064012, 2016.

[8] D. Zhang *et al*., "Combination of advanced optical modeling with electrical simulations for performance evaluation of practical 4-terminal perovskite/silicon tandem modules," *Energy Procedia*, vol. 92, pp. 669-677, 2016.

[9] M.A. Green *et al.*, "Solar cell efficiency tables (version 50)", *Prog. Photovolt. Res. Appl.*, vol. 25, p. 668-676, 2017.

[10] K. Yoshikawa *et al*., "Silicon heterojunction solar cell with interdigitated back contacts for a photoconversion efficiency over 26%," *Nature Energy*, vol. 2, 17032, 2017.

[11] M.A. Green *et al*., "Solar cell efficiency tables (version 51)," *Prog. Photovolt. Res. Appl.*, vol. 26, pp. 3-12, 2018.

[12] W.S. Yang *et al.*, "Iodide management in formamidinium-lead-haldide-based perovskite layers for efficient solar cells," *Science*, vol. 356, pp. 1376-1379, 2017.

[13] S. Albrecht *et al*., "Monolithic perovskite/silicon heterojunction tandem solar cells processed at low temperature," *Energy Environ. Sci*., vol. 9, pp. 81-88, 2016.

[14] K.A. Bush *et al*., "23.6%-efficient monolithic perovskite/silicon tandem solar cells with improved stability", *Nature Energy*, vol. 2, 17009, 2017.

[15] F. Sahli, J. Werner *et al*., "Fully textured monolithic perovskite/silicon tandem solar cells with 25.2% power conversion efficiency", *Nature Materials*, vol. 17, pp. 820-826, 2018.

[16] https://www.oxfordpv.com/news/oxford-pv-sets-world-record-perovskite-solar-cell.

[17] T. Duong *et al.*, "Rubidium multication perovskite with optimized bandgap for perovskite-silicon tandem with over 26% efficiency," *Advanced Energy Materials*, vol. 7, 1700228 (2017).

[18] C.O. Ramirez Quiroz *et al.*, *J. Mater. Chem. A*, vol. 6, pp 3583-3592, 2018.

[19] H. Uzu *et al.*, "High-efficiency solar cells combining a perovskite and a silicon heterojunction solar cells via an optical splitting system," *Appl. Phys. Lett.*, vol. 106, 013506, 2015.

[20] M. Rienacker *et al*., "Maximum power extraction enabled by monolithic tandems using interdigitated back contact bottom cells with three terminals," *33rd EUPVSEC Amsterdam*, 2017.

[21] G.W.P. Adhyaksa, E. Johlin, and E.C. Garnett, "Nanoscale back contact perovskite solar cell design for improved tandem efficiency," *Nano Lett.*, vol. 17, pp. 5206-5212, 2017.

[22] K. Yoshikawa *et al.*, "6 inch high efficiency back contact crystalline Si solar cell applying heterojunction and thinfilm technology," *Proceedings of 43rd IEEE PVSC, Portland, US*, pp. 3366-3369, 2016.

[23] R. Santbergen *et al.*, "GenPro4 optical model for solar cell simulation and its application to multijunction solar cells," *IEEE J. Photovolt*., vol. 7, p.919-926, 2017.

[24] P. Loper *et al.*, "Organic-inorganic halide perovskite / crystalline silicon four-terminal tandem solar cells," *Phys. Chem. Chem. Phys.*, vol. 17, pp. 1619-1629, 2015.

[25] D. Zhang *et al.*, "Design and fabrication of SiOx/ITO double-layer anti-reflection coating for heterojunctin silicon solar cells," *Sol. Energ. Mat. Sol. Cells*, vol. 117, pp. 132-138, 2013.

[26] A.H.M. Smets *et al*., "Solar energy: the physics and engineering of photovoltaic conversion technologies and systems," UIT Cambridge 2016.

[27] http://ngspice.sourceforge.net

[28] K. Jager, L. Korte, B. Rech, and S. Albrecht, "Numerical optical optimization of monolithic planar perovskite silicon tandem solar cells with regular and inverted device architectures," *Opt. Express*, vol. 25, A473-A482, 2017.

[29] R. Santbergen *et al.*, "Minimizing optical losses in monolithic perovskite / c-Si tandem solar cells with flat top cell," *Opt. Express*, vol. 24, A1288-A1299, 2016.

[30] H. Tan, P. Babal, M. Zeman, and A.H.M. Smets, "Wide bandgap p-type nanocrystalline silicon oxide as window layer for high performance thin-film silicon multijunction solar cells," *Sol. Energy Mater. Sol. Cells*, vol. 132, pp. 597-605, 2015.

[31] L. Mazzarella et al., "Infrared photocurrent management monolithic perovskite / silicon heterojunction tandem solar cells by using a nanocrystalline silicon oxide interlayer," Optics Express, vol. 26, A487-A497, 2018.

[32] F. Sahli *et al.*, "Improved optics in monolithic perovskite/silicon tandem solar cells with a nanocrystalline silicon recombination junction," *Advanced Energy Materials*, vol. 8, 1701609, 2018.